Functional imaging of cerebrovascular activities in small animals using high-resolution photoacoustic tomography

Sihua Yang and Da Xing[a)]
MOE Key Laboratory of Laser Life Science and Institute of Laser Life Science, South China Normal University, Guangzhou 510631, China

Quan Zhou
Medical Imaging Center, First Affiliated Hospital of Jinan University, Guangzhou 510630, China

Liangzhong Xiang and Yeqi Lao
MOE Key Laboratory of Laser Life Science and Institute of Laser Life Science, South China Normal University, Guangzhou 510631, China

(Received 20 March 2007; revised 4 June 2007; accepted for publication 5 June 2007; published 25 July 2007)

Photoacoustic imaging (PAI) is a noninvasive, nonionizing modality based on the differences in light absorption of various biological tissues. PAI utilizes the endogenous contrast characteristics of traditional optical imaging, while benefiting from high spatial resolution of the ultrasound imaging. A PAI system was developed to reconstruct the two-dimensional cross section image and to visualize the cerebrovascular activities of mouse *in vivo*. The spatial resolution of the PAI system was determined to be 0.110 mm by a two-point-source phantom with the Rayleigh criterion. The potential applications of the system were clearly demonstrated by successfully mapping a traumatic lesion in the mouse brain cerebral cortex, by its ability to monitor physiological changes in the brain due to carotid ligation and drug stimulation, and two-dimensional sliced images of a traumatic mouse brain at different depths were also provided. Our experimental results indicate that PAI has the potential for studying of traumatic brain injury and physiological functions of the brain. © *2007 American Association of Physicists in Medicine*. [DOI: 10.1118/1.2757088]

Key words: photoacoustic imaging, photoacoustic signal, brain vascular, traumatic lesion, drug stimulation

I. INTRODUCTION

Cerebrovascular disease occurs when blood vessels supplying the brain with oxygenated blood are damaged. Two primary pathophysiologic features of cerebrovascular diseases are the interruption of blood flow to part of the brain and the rupture of blood vessels, resulting in bleeding in the cerebral parenchyma. Cerebrovascular disease can cause stroke when there is a sudden blockage or rupture of a blood vessel within the brain. If the flow of blood in an artery supplying the brain is interrupted for longer than a certain period, brain cells can die, causing permanent damage. Survivors of cerebrovascular disease often suffer a residual neurologic deficit and require chronic care.[1–3]

The brain microvasculature plays an important role in brain function and metabolism. However, the etiology of many cerebrovascular diseases is poorly understood. A technique that would accurately monitor brain blood activities would be of a great value for studying cerebrovascular diseases. Various methods are being explored for functional imaging of cerebrovascular activities, such as single photon emission computed tomography (SPECT), positron emission tomography (PET), and magnetic resonance imaging (MRI). SPECT and PET rely on a family of tracer methods for measuring different physiological quantities such as blood volume, blood flow, and regional oxygen extraction.[4] Functional MRI, based on blood oxygenation level-dependent (BOLD) contrast, can detect changes in hemodynamics. However, the resolution of these modalities is too poor to satisfy the functional mapping of microvasculature in the cerebral cortex for basic research. Other shortcomings of the current imaging modalities are their high cost and large size. Therefore, novel functional imaging of microvasculature is much needed for detecting cerebrovascular dysfunction and monitoring the pathogenic process.

A photoacoustic (PA) signal is the result of photothermal effects. When biological tissue is irradiated with a laser pulse of adequate energy, a small temperature rise in the tissue causes a rapid thermal expansion that leads to the emission of a thermoelastic sound wave. By detecting the sound wave on the tissue surface and via signal reconstruction,[5–12] photoacoustic imaging (PAI) provides the distribution of absorbed optical energy density inside the target tissue.[13–16] It has been shown as a powerful tool for visualizing biological tissues with high optical contrast and high ultrasonic resolution.[17–22] The technique has been used to determine vessel diameter in rabbits[23] and to measure burn depth in rats.[24] Compared with the existing pure optical imaging modalities such as diffuse optical tomography, optical coherence tomography, and fluorescence imaging, PAI overcomes the overwhelming scattering of light in biological tissues by utilizing ultrasonic waves to express the absorbed optical energy deposit information, thus providing higher spatial resolution with depth.[25] The available high contrast related to the

optical properties of biological tissues in visible or near-infrared (NIR) regions of the electromagnetic spectrum can be used in determining tissue structures and disorders.

Changes in the optical properties of cerebral tissue are often caused by variations in cerebral blood flow (volume), oxygen consumption, and oxygen saturation, which are often associated with brain physiology and pathology.[26–29] This association is the basis for evaluating physiological and functional properties of the brain. Based on the intrinsic optical absorption of biological tissues, PAI can provide a noninvasive method to map and monitor changes in cerebral cortical vasculature with high contrast and high spatial resolution. Although it is very difficult to image human brain directly with PAI at present, the PA imaging of microvasculature in the mouse brain model can provide more knowledge and information of cerebrovascular diseases. An article on the monitoring of cortical neural activities in response to whisker stimulation by the PA technique has been reported.[30]

In this article, we emphasize the demonstration of PAI monitoring of different pathology models in the mouse brain. A PAI system was designed and developed to further study applying the PA technique for functional brain imaging. The system was applied to acquire *in vivo* images of the mouse brain suffering either a cortical trauma or a carotid artery occlusion. It was also used to monitor the physiological changes in the brain caused by drug stimulation. Two-dimensional slices of a traumatic mouse brain were also obtained.

II. MATERIALS AND METHODS

A. PAI principle and image reconstruction

PA source wave can be generated when optical energy pulses are delivered to a target tissue. The strength of the PA source wave is proportional to the locally absorbed energy density. When optical energy is delivered in a pulse that is short enough so that thermal diffusion can be ignored, the resulting PA pressure $p(r,t)$ that reaches a detector at position r and time t can be expressed as[22,31]

$$p(r,t) = \frac{I_0 \beta}{4\pi C_p} \int\int\int \frac{d^3(r')}{|r-r'|} A(r') T'(t'), \tag{1}$$

where β is the isobaric volume expansion coefficient, C_p is the specific heat, I_0 is a factor proportional to the incident optical energy density, $T'(t')$ denotes the temporal profile of the light with units of $1/s$, which can be regarded as a Dirac delta function $\delta(t)$ for a short laser pulse, and $A(r')$ is the absorbed optical energy deposition per unit volume of soft tissue at position r'.

The PA source wave propagates from its originating region and can be detected by an ultrasonic transducer or an array detector. The objective of PAI is to determine the distribution of absorbed optical energy $A(r')$ in a target tissue through a reconstruction algorithm, from a set of measured PA signals $p(r,t)$. In the current study, a modified filtered back-projection algorithm[9] developed by our early work is used to reconstruct the distribution of absorbed optical energy density. This algorithm allows the absorbed optical energy density of a target to be reconstructed by deconvolving the recorded PA signals from a point source, and without measuring the impulse response of the transducer. The PA signals from a point source can be easily obtained by focusing the incident laser on an absorber surface to form a point source.

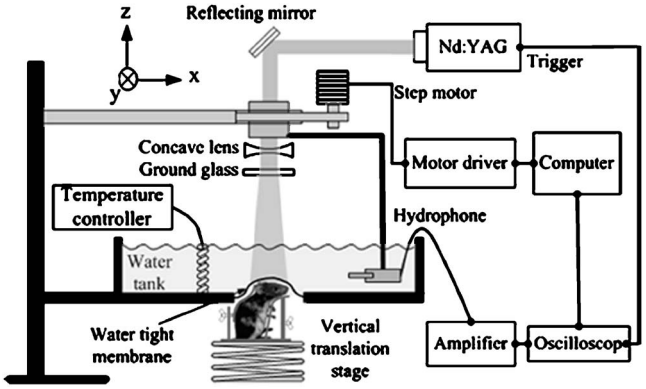

FIG. 1. PAI system for noninvasive imaging of mouse brain.

B. PAI system for noninvasive imaging of mouse brain *in vivo*

The schematic of the PAI system for animal brain imaging is shown in Fig. 1. An Nd: YAG laser (LS-2134, LOTIS TII, Belarus) was employed to produce 532 nm laser pulses (pulse width, 10 ns; repetition rate, 15 Hz) for generating PA signals. The 532 nm wavelength was selected because of its prominent high absorption by blood (hemoglobin). The laser beam was expanded by a concave lens and then homogenized with a ground glass. The light then irradiated onto the mouse brain and the diameter of the beam is approximately 1.3 cm. The incident energy density on the brain surface was set at 8 mJ/cm^2. A needle hydrophone (Precision Acoustics Ltd, Dorchester, UK; diameter, 1 mm; sensitivity, 850 nv/Pa; frequency response, 200 KHz to 15 MHz) was used to receive the PA signals. A custom-built water tank coupled the PA signals between the hydrophone and the mouse head. The hydrophone was controlled by a precise stepper motor to scan circularly around the mouse head in the horizontal plane ($X-Y$ plane). To cover a 2π receiving angle for imaging the mouse brain, a total of 200 steps with a constant 1.8° interval were taken, where the radius of the circular scan was about 4 cm. The PA signals acquired from the hydrophone were amplified and then recorded with a digital oscilloscope (TDS3032, Tektronix, Beaverton, OR, USA) at a sampling rate of 500 Msamples/s. At each sampling position, the PA signal was averaged for 64 traces. A complete circular scan required approximately 15 min. Finally, the computer acquired all of the amplified and digitized data and reconstructed the distribution of absorbed optical energy density in the imaging plane. The ultrasound speed is assumed to be exactly 1500 m/s for every PA reconstructed image.

C. Animal model

BALB/c mice (both genders, 25–35 g body weight) were used for the PAI experiments. Before imaging, the fur over the skull of mice was shaven and chemically depilated. General anesthesia (i.p. sodium pentobarbital, 40 mg/kg; supplemental, 10 mg/kg/h or as necessary) was administered to keep the mice motionless throughout the experiment.

The anesthetized mouse was placed on a vertical adjustable pad with a custom-stereotactic head holder. The mouse head protruded into the water tank through a hole at the bottom of the tank under a piece of clear membrane. A thin layer of ultrasonic coupling gel was applied to the surface of the animal head to couple the head and the flexible membrane at the bottom of the water tank. A temperature controller was used to keep the temperature of the water at 37 °C.

D. Brain trauma induction

The surface of the head was disinfected with alcohol. A sterile steel needle with a diameter of 0.3 mm was inserted into the right cerebral cortex through the skin and the skull to induce a cortical lesion and cerebral hemorrhage. The brain was mapped with PAI immediately. A control image of the brain was acquired before the induction of brain lesions. Upon completion of the imaging process, the mouse was sacrificed and an open-skull photograph of the cerebral cortex was taken.

E. Cerebral ischemia induction

The left common carotid artery was exposed through a small midline incision on the neck, and then was meticulously isolated from the surrounding tissues using microsurgical instruments. Finally, it was tightened with an overhand knot suture to disrupt the blood flow and form the regional cerebral ischemia.[32] The mouse was immediately imaged by the PAI system. After each experiment, the overhand knot suture in the mouse was loosened, the incision closed, and the animal was allowed to recover.

F. Drug stimulation

Acetazolamide (ACZ) is a carbonic anhydrase inhibitor that increases cerebral blood flow (CBF) and induces dilatation of the cerebral microvasculature,[33–35] while leaving cerebral metabolic rate for oxygen unchanged.[36] The functional imaging of blood activities in the mouse brain cortex in response to the drug (ACZ) was investigated by the potential PA technique. The mouse was tube fed with ACZ (400 mg/kg) via the esophagus. The effects of ACZ in the mouse could be maintained for up to about 3 h.[37] The mouse was imaged before and after the administration of ACZ. After the experiment, the mouse recovered normally without noticeable health problems.

G. Tomographic images at different depths

To obtain vertical slice tomographic images of a traumatic mouse brain at different depths, the hydrophone was fixed on a translation stage for scanning along the Z axis with a step size of 1 mm. A cylinder acoustic lens made of polymethylmethacrylate (focal length, 1.5 cm) was placed in front of the needle hydrophone in order to suppress out-of-plane signals and improve the tomographic ability. At each depth in the Z axis, the needle hydrophone scanned around the mouse head in horizontal plane for two-dimensional (2D) cross sectional imaging.

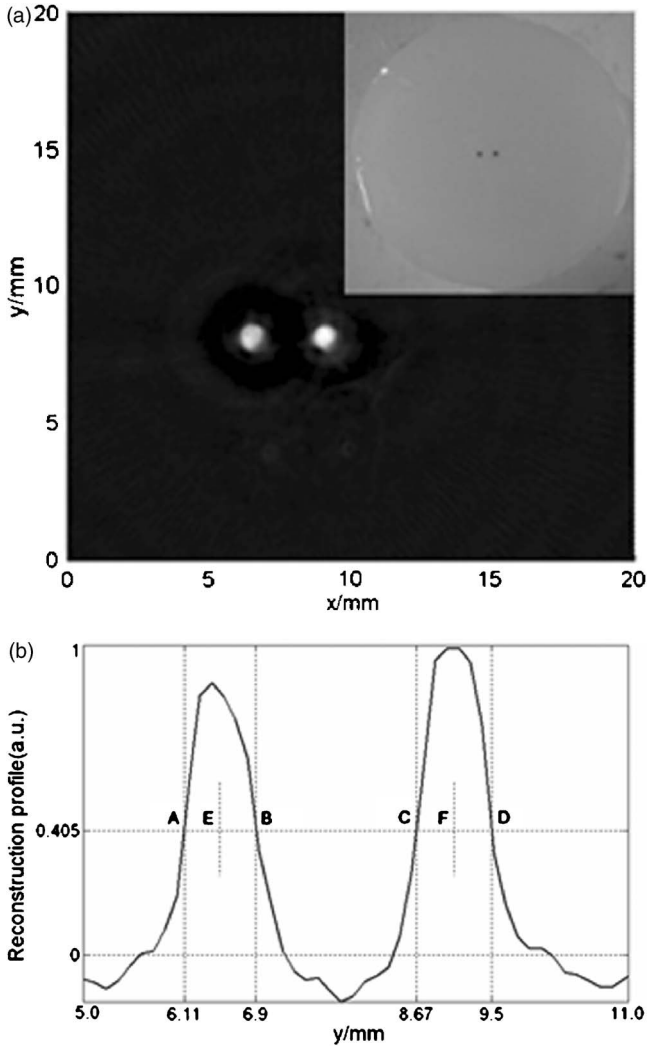

FIG. 2. Spatial resolution of the PAI system. (a) PA image of a cross section of a two-carbon-rods phantom. The two carbon rods (diameter 0.7 mm) are embedded in the cylindrical phantom at a depth of 2 mm. The center distance between the two graphite rods is 2.5 mm. The insert at the top-right corner is the photograph of the phantom. (b) Line profile of the reconstructed image shown in (a) with $y=8.1$ mm.

III. RESULTS

A. Spatial resolution of the PAI system

To evaluate the image resolution of this PAI system, we imaged two carbon rods (0.7 mm in diameter) fixed in a phantom (15% gelatin, 12.5% milk, and 74.5% water), which was used to simulate the optical properties of human tissue. The carbon rods were placed in rotation center and imaged

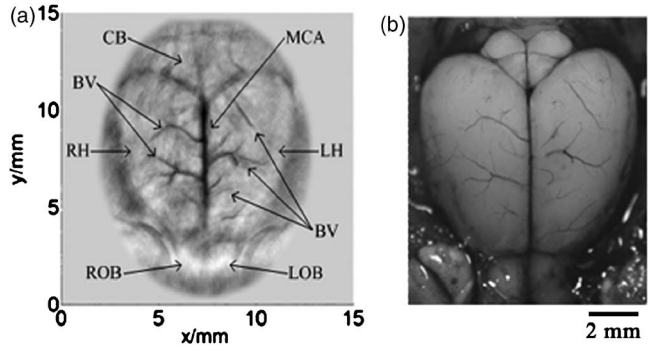

FIG. 3. PA images of mouse brain *in vivo*. (a) Noninvasive image of a mouse brain acquired using the PAI system with the skin and skull intact. Detailed brain tissue structures: CB, cerebellum; BV, blood vessel; LH, left hemisphere; LOB, left olfactory lobe; MCA, middle cerebral artery; RH, right hemisphere; and ROB, right olfactory lobe. (b) Open-skull photograph of the mouse brain surface acquired postmortem.

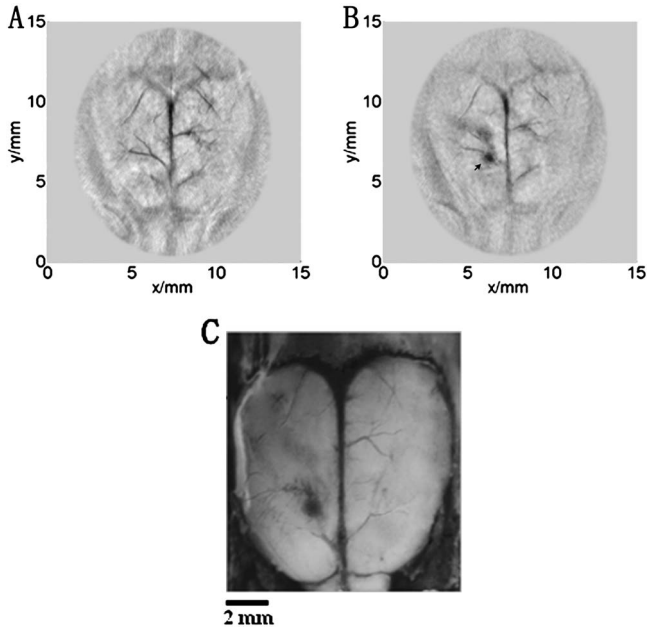

FIG. 4. PA images of traumatic lesion. (a) PA image of the brain before induction of lesions. (b) PA image of a needle-induced superficial lesion (in the right cerebral cortex, identified by the arrows) and cerebral hemorrhage (around the lesion areas) on the mouse brain. (c) Open-skull photograph of the mouse cerebral surface acquired after the imaging experiment.

with the PAI system. Figure 2(a) shows the PA reconstructed image of the phantom with two inserted carbon rods. Figure 2(b) is the normalization line profile of the reconstructed image shown in Fig. 2(a) with $y=8.1$ mm. The profile includes two absorption sources. The 40.5%-amplitude line intercepts with the profile at points A, B, C, and D, and it also intercepts with the centerlines of the two absorption peaks at points E and F, respectively [Fig. 2(b)]. The spatial resolution of the system is estimated according to the Rayleigh criterion. The two sources can no longer be clearly distinguished when point B touches point C in Fig. 2(b). Therefore, the minimum distinguishable distance, R, between the two sources is approximately $R=|EB|+|CF|-2r$, where r is the radius of the absorption source. From Fig. 2(b), the R is measured to be ~0.110 mm. The image resolution of the circular scanning system will deteriorate with an increase in distance from the center of rotation owing to the aperture effect. Therefore, the spatial resolution of the imaging system in the central area with the diameter of ~6 mm is determined to be ~0.110 mm.

B. PAI of normal mouse brain *in vivo*

A PA image of a mouse brain acquired noninvasively with the skin and the skull intact is shown in Fig. 3(a). The PA reconstructed image corresponds to the cortical surface of the mouse brain, where the vascular distribution is evidently visualized. Owing to the different optical absorptions between blood vessels and the background parenchyma, the major characteristic tissue structures in mouse brain are clearly distinguished. The vascular network of the PA reconstructed image is in excellent agreement with the open-skull anatomical photograph [Fig. 3(b)]. This experiment testified that PAI has the ability for noninvasively imaging of brain cortical vasculature.

C. Detection of traumatic brain lesions

The PA images of the mouse cerebral cortex, before and after the induction of needle-induced lesion, are shown in Figs. 4(a) and 4(b), respectively. A region with increased optical absorption corresponding to the traumatic lesion region is clearly shown in Fig. 4(b). Compared with its anatomical photograph [Fig. 4(c)], the disruption of the vessels in the right cerebral cortex was unequivocally detected with PAI and matched well both in position and shape. The images suggest that PAI can detect not only the intrinsic cerebral vasculature, but also the brain hemorrhage caused by trauma. The brain trauma images from PAI provide the information on physiological changes in addition to morphologic observation in the brain.

D. Monitoring of brain ischemia

A mouse brain was imaged noninvasively with the PAI system before and after its left carotid artery was occluded. On a gray scale, where darker areas represent higher absorbed optical energy, the images clearly show a diminished blood volume pattern after carotid artery occlusion. A rectangular region in the left cerebral cortex was selected, as marked with a dotted frame in the images of Figs. 5(a) and 5(b), corresponding to the anticipated ischemia during the carotid occlusion. Compared with the preocclusion image in Fig. 5(a), the image in Fig. 5(b) represents a clear map of local ischemic region, where the blood vessels provided a weak PA signal. The decrease in signal intensity of the blood vessels within the dotted frame primarily resulted from the decline of blood flow and blood volume. Hence, amplitude differences as displayed by the images indicate real changes in signal strength. The observed fractional change in absorbed optical energy density, A'/A [A and A' are the optical absorptions per unit volume before and after artery occlusion, respectively, as described in Eq. (1)] in the blood ves-

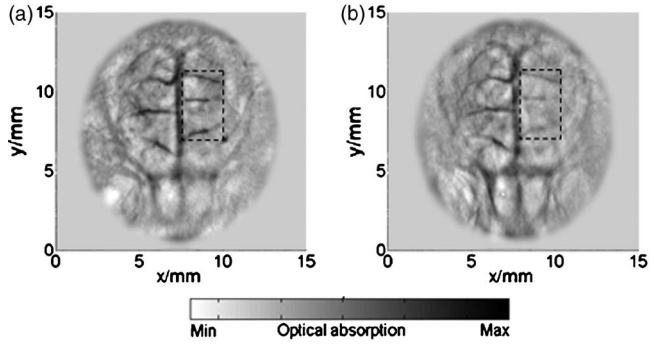

FIG. 5. PA monitoring of cerebrovascular occlusion. (a) PA image of brain cerebral cortex surface before carotid ligation. (b) PA image of brain cerebral cortex surface during carotid artery occlusion. Dotted frame corresponds to the anticipated ischemic region.

sels within the dotted frame was on average reduced by 65% after the artery occlusion. The images and the regional changes of the PA signal intensity strongly suggest that brain blood vessel occlusion can be monitored with the PAI system. After the imaging experiment, a phenomenon of hemiplegy of the right limbs of the mouse was found after its recovery from anesthesia. This is consistent with brain function: The symptoms are usually on the side of the body opposite to the side of the brain where the damage has occurred.

E. Response of cortical vessels during drug stimulation

The PAI system was also used to monitor the brain cortical vessels in response to the changes of CBF due to drug (ACZ) stimulation. Two subsequent PA images of the cortical vasculature were obtained on the same mouse brain without and during ACZ stimulation [Figs. 6(a) and 6(b), respectively]. When the ACZ acted on the brain, the dilation of the major vessel branches could be observed on the PA reconstructed images. By comparing the two images, it is apparent that some detailed vascular structures that are difficult to visualize from the image in Fig. 6(a), such as the small vessel branches identified by the black arrowheads in the figure, can be seen clearly during the drug stimulation in Fig. 6(b). According to the gray scale, the slightly increased signal intensity of the blood vessels in Fig. 6(b) likely resulted from the increase of CBF causing by the ACZ stimulation. Moreover, the diameter changes of the cerebrovasculature can be observed by visualizing the reconstructed PA images and analyzing the signal profile. The corresponding PA intensity profiles along the lines shown in Figs. 6(a) and 6(b) were evaluated and plotted in Fig. 6(c). The lines were drawn through two major blood vessels of interest, with the peaks likely due to the higher optical absorption of the vessels. The diameters of the blood vessels were obviously expanded due to ACZ stimulation and could be estimated from the full widths at half-maximum (FWHM) of the PA signal profiles. Using the above method, we measured diameters of different blood vessels (from 80 to 200 μm) before and during drug stimulation and found the averaged dilation of the vessel

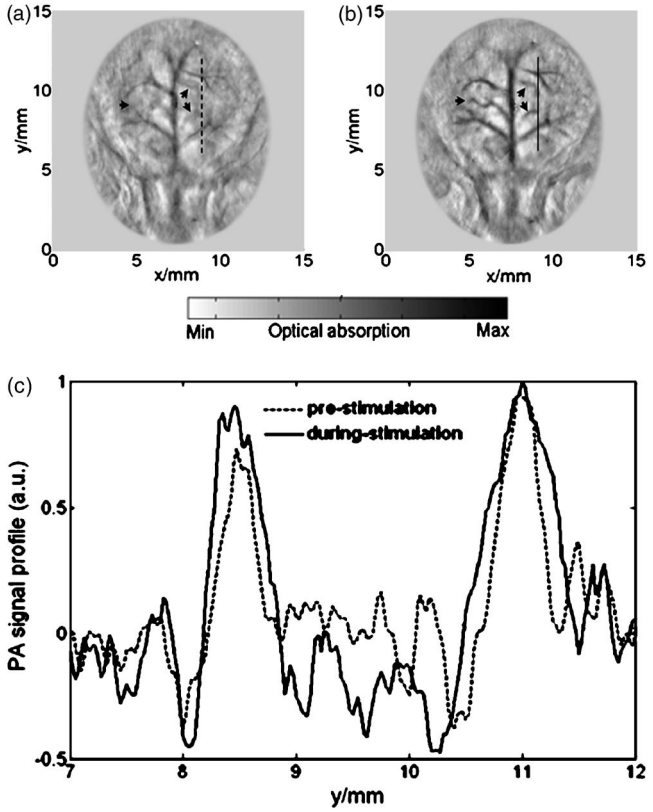

FIG. 6. Cerebral hemodynamic changes in response to drug stimulation. (a) Noninvasive PA image of the vasculature in the superficial layer of the mouse cortex acquired without drug stimulation. (b) Noninvasive PA image of the vasculature in the superficial layer of the mouse cortex acquired during drug (acetazolamide) stimulation with several small blood vessels of interest identified by arrowheads. (c) Signal intensity profiles along the lines marked in (a) and (b) [dashed profile corresponds to the dashed line outlined in (a), and the solid profile corresponds to the solid line outlined in (b)].

diameters to be 38% ±5% upon drug stimulation. These experimental results demonstrate the feasibility of PAI to access the information of cerebrovascular activities in response to drug stimulation.

F. Tomographic images of a traumatic mouse brain

The traumatic injury in a mouse brain cortex at different depths was successfully measured by combining circular scanning on the $X-Y$ plane with vertical scanning along the Z axis. PA tomographic slices of optical absorption in the horizontal cross sections at different depths (layers) are shown in Figs. 7(a)–7(d). From the reconstruction image of 0.5 mm depth [Fig. 7(a)], a clear distribution of the superficial blood vasculature in the cerebral cortex was acquired as well as the trauma lesion and the accompanying hemorrhage. The gray scale in all the PA images refers to the same range of absolute values. Hence, the changes of signal strength as displayed by the images represented the real absorbed optical energy deposit, which implied the changes of blood (hemoglobin) distribution at different depths. Therefore, the images in Figs. 7(b)–7(d) reflected the interior brain structures underneath the superficial cortex and the needle-induced lesion

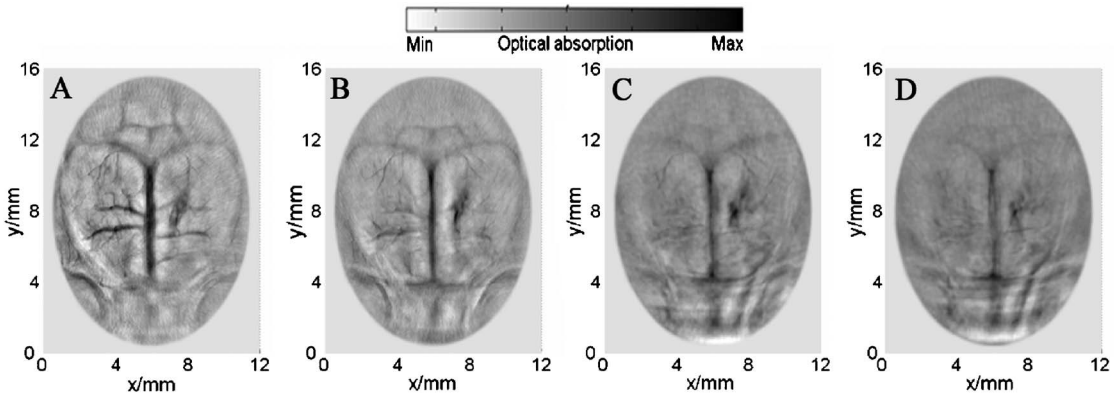

FIG. 7. PA tomography of mouse brain with a needle-induced lesion. The images were reconstructed for horizontal cross sections of the mouse brain at different depths: (a) 0.5 mm; (b) 1.5 mm; (c) 2.5 mm; and (d) 3.5 mm from the top surface of the mouse's head.

with sufficient clarity up to a 3.5 mm depth. This result indicates that PAI may used to acquire the depth information of a lesion.

IV. DISCUSSION

Microvascular imaging technologies may provide a much needed tool for basic research of the cerebrovascular diseases and the brain hemodynamics. The absorption coefficient of whole blood (>100 cm^{-1} at 532 nm) is much higher than the average absorption coefficient of gray and white matter of the brain (~ 0.56 cm^{-1} at 532 nm).[38] If the incident optical energy density and the structure of the absorbing object remain unchanged, the intensity of the PA signals produced by the object is proportional to its optical absorption coefficient.[39–41] PAI with high-resolution mapping of the tissue absorbed optical energy distribution is an excellent technique for blood distribution in cerebral cortex. Compared to the former study,[30,39] our present results further exploit the potential new application of the PA technique and demonstrate the noninvasive detection of traumatic lesions and monitoring of the cerebrovascular changes due to the external physiological interference. It is anticipated that this technique may be used for studying and diagnosing a number of diseases and visualizing tumor growth and trauma brain injury rehabilitation in the pathogenic process.

Full-view circular-scan geometry and the modified back-projection algorithm were employed in our experiments. The superficial mapping of the absorbed optical energy density in the brain cerebral cortex can be accurately reconstructed from the detected PA signals. The spatial resolution of the PAI system is primarily limited by the bandwidth of the detected PA signals rather than by optical diffusion as in conventional optical imaging. The spatial resolution of the current imaging system in the central area (diameter, 6 mm) was determined to be 0.110 mm [Fig. 2(b)]. However, small movements due to the breathing of the animal may influence the spatial resolution. Moreover, the homogeneity of the laser beam can be influenced when light penetrates the skin and the skull; this may also produce unwanted errors when interpreting the distribution of absorbed optical energy density. Understanding and minimizing these problems are central parts of our future work to further increase the spatial resolution of the PAI systems.

Animal models for cerebrovascular diseases, such as traumatic brain injury, brain hemorrhage, and acute ischemic stroke, provide us with knowledge about the causes, diagnosis, and therapy of these diseases. In our experiments, the *in vivo* imaging of mouse brain structures as well as vascular distribution is achieved noninvasively, as shown in Fig. 3. The accurate mapping of the brain lesions and local cerebral ischemia, as shown in Figs. 4 and 5, demonstrated the clinical potential of PAI. This imaging technique can be expanded to monitor different stages of disease and developmental changes by a series of PA images taken over time, enabling a more comprehensive description of the pathologic state of cerebrovascular diseases.

Optical measurement of the brain is desirable due to its functionality.[42–44] Brain physiology and pathology are associated with optical properties such as the absorption and scattering of brain tissues.[26] Conventional optical modalities for functional imaging, however, have serious drawbacks due to the overwhelming scattering of light in biological tissue. The PA technique, with its unique characteristics, can provide satisfactory imaging quality on the vasculature of mouse brain.

The stimulation of cerebral perfusion on the mouse was performed by ACZ injection, and the images of stimulated brain were acquired in our experiments, as shown in Fig. 6. We found that vessel diameter was noticeably dilated compared with that of the control. Thus, this technique can provide information on blood activities indirectly by monitoring the changes in vessel diameter. The study of functional changes in regional CBF is of great significance for diagnostic imaging and therapeutic monitoring. The PAI technique is likely to make efforts to the study of regional brain activity.

In our study, the circular scan in the $X-Y$ plane in combination with the linear scan along the Z axis constituted a cylindrical scan around the mouse head. PA signals were acquired and reconstructed to form the 2D images of multiple cross sections at different depths, as shown in Fig. 7. The resolution in the $X-Y$ plane is high, but the resolution

along the *Z* axis is limited [Figs. 7(b) and 7(d)] and is primarily dependent on the wide acceptance angle and the element size along the *Z* axis of the transducer. Though a cylinder lens was use to select the 2D imaging plane, the reconstructed images of the mouse brain at different depths still are superposition images of certain thickness, projected along the direction of the laser beam onto the observation cross section. A transducer with built-in cylindrically focused lens or a 3D reconstruction algorithm can be used to improve the elevation resolution.

One limitation of this system is the relatively long scanning time. A reduction of the scanning time can be realized by using a multielement transducer array[45,46] instead of a rotating single-element transducer and by using a laser with a higher pulse repetition rate. The present imaging depths are largely limited by the 532 nm laser light delivery. It is promising for the PA technique to image the neonatal brain when NIR is applied to help great depths.

Since the brain is highly responsive to changes in the blood oxygenation level, the application of PAI will be greatly broadened when multiple wavelengths are employed to obtain oxygen-dependent imaging, as demonstrated by the pioneer work.[39] PA imaging employing multiple wavelengths may evaluate hemodynamic changes in the brain such as hemoglobin concentration and blood oxygen saturation, which can potentially help quantify the hyperemic and hypoxia in the brain. Furthermore, with the use of exogenous contrast agents,[47,48] such as specific agents with capabilities of targeting tumor cells, PAI can be used for early tumor detection and molecular imaging.

In summary, we have developed a noninvasive PAI system, based on physiology-dependent intrinsic signal changes, for brain therapeutic monitoring and functional mapping. Our *in vivo* imaging results using a mouse model suggest that PAI can be used for mapping cerebral vasculature and for monitoring cerebrovascular changes in response to physiological interference. Therefore, the photoacoustic technique has the potential to be widely applied in neurophysiology, neuropathology, and neurotherapy.

ACKNOWLEDGMENTS

This research was supported by the National Natural Science Foundation of China (Grant Nos. 60678050; 30470494; 30627003) and the Natural Science Foundation of Guangdong Province (Grant No. 015012). We would like to thank Professor Huamin Gu for useful discussions and suggestions. We also acknowledge the technical asistance by Dr. Diwu Yang and Dr. Lvming Zeng.

[a]Author to whom correspondence should be addressed. Electronic mail: xingda@scnu.edu.cn

[1]D. M. Bravata, S. Y. Ho, L. M. Brass, J. Concato, J. Scinto, and T. P. Meehan, "Long-term mortality in cerebrovascular disease," Stroke **34**, 699–704 (2003).
[2]F. Vernieri, P. Pasqualetti, M. Matteis, F. Passarelli, E. Troisi, P. M. Rossini, C. Caltagirone, and M. Silvestrini, "Effect of collateral blood flow and cerebral vasomotor reactivity on the outcome of carotid artery occlusion," Stroke **32**, 1552–1558 (2001).
[3]J. Vijungco and M. K. Eskandari, "New treatments for cerebrovascular disease," Perspect. Vasc. Surg. Endovasc. Ther. **17**, 279–287 (2005).
[4]R. M. Dijkhuizen, J. Ren, J. B. Mandeville, O. Wu, F. M. Ozdag, M. A. Moskowitz, B. R. Rosen, and S. P. Finklestein, "Functional magnetic resonance imaging of reorganization in rat brain after stroke," Proc. Natl. Acad. Sci. U.S.A. **98**, 12766–12771 (2001).
[5]G. Paltauf, J. A. Viator, S. A. Prahl, and S. L. Jacques, "Iterative reconstruction algorithm for optoacoustic imaging," J. Acoust. Soc. Am. **112**, 1536–1544 (2002).
[6]P. Liu, "The P-transform and photoacoustic image reconstruction," Phys. Med. Biol. **43**, 667–674 (1998).
[7]S. J. Norton and T. Vo-Dinh, "Optoacoustic diffraction tomography: Analysis of algorihms," J. Opt. Soc. Am. A **20**, 1859–1866 (2003).
[8]Z. Yuan and H. Jiang, "Three-dimensional finite element-based photoacoustic tomography: Reconstruction algorithm and simulations," Med. Phys. **34**, 538–546 (2007).
[9]Y. Wang, D. Xing, Y. Zeng, and Q. Chen, "Photoacoustic imaging with deconvolution algorithm," Phys. Med. Biol. **49**, 3117–3124 (2004).
[10]R. A. Kruger, D. R. Reinecke, and G. A. Kruger, "Thermoacoustic computed tomography-technical considerations," Med. Phys. **26**, 1832–1837 (1999).
[11]M. Xu and L. V. Wang, "Time-domain reconstruction for thermoacoustic tomography in a spherical geometry," IEEE Trans. Med. Imaging **21**, 814–822 (2002).
[12]M. Xu, Y. Xu, and L. V. Wang, "Time-domain reconstruction-algorithms and numerical simulations for thermoacoustic tomography in various geometries," IEEE Trans. Biomed. Eng. **50**, 1086–1099 (2003).
[13]J. J. Niederhauser, M. Jaeger, R. Lemor, P. Weber, and M. Frenz, "Combined ultrasound and optoacoustic system for real-time high-contrast vascular imaging *in vivo*," IEEE Trans. Med. Imaging **24**, 436–440 (2005).
[14]Z. Yuan, H. Z. Zhao, C. F. Wu, and H. B. Jiang, "Quantitative imaging of small nanoparticle-containing objects using finite element-based photoacoustic tomography," Opt. Lett. **30**, 3054–3056 (2005).
[15]C. G. A. Hoelen, F. F. de Mul, R. Pongers, and A. Dekker, "Three-dimensional photoacoustic imaging of blood vessels in tissue," Opt. Lett. **23**, 648–650 (1998).
[16]A. A. Karabutov, E. Savateeva, and A. Oraevsky, "Imaging of layered structures in biological tissues with opto-acoustic front surface transducer," Proc. SPIE **3601**, 284–295 (1999).
[17]R. I. Siphanto, K. K. Thumma, R. G. M. Kolkman, T. G. v. Leeuwen, F. F. M. d. Mul, J. W. v. Neck, L. N. A. v. Adrichem, and W. Steenbergen, "Serial noninvasive photoacoustic imaging of neovascularization in tumor angiogenesis," Opt. Express **13**, 89–95 (2005).
[18]Y. Zeng, D. Xing, Y. Wang, B. Yin, and Q. Chen, "Photoacoustic and ultrasonic coimage with a linear transducer array," Opt. Lett. **29**, 1760–1762 (2004).
[19]X. Wang, Y. Pang, G. Ku, G. Stoica, and L. V. Wang, "Three-dimensional laser-induced photoacoustic tomography of mouse brain with the skin and skull intact," Opt. Lett. **28**, 1739–1741 (2003).
[20]L. Xiang, D. Xing, H. Gu, D. Yang, S. Yang, L. Zeng, and W. R. Chen, "Real-time optoacoustic monitoring of vascular damage during photodynamic therapy treatment of tumor," J. Biomed. Opt. **12**, 014001–014008 (2007).
[21]L. Zeng, D. Xing, H. Gu, D. Yang, S. Yang, and L. Xiang, "High antinoise photoacoustic tomography based on a modified filtered backprojection algorithm with combination wavelet," Med. Phys. **34**, 556–563 (2007).
[22]M. Xu and L. V. Wang, "Photoacoustic imaging in biomedicine," Rev. Sci. Instrum. **77**, 041101–041123 (2006).
[23]R. G. Kolkman, J. H. Klaessens, E. Hondebrink, J. C. Hopman, F. F. de Mul, W. Steenbergen, J. M. Thijssen, and T. G. van Leeuwen, "Photoacoustic determination of blood vessel diameter," Phys. Med. Biol. **49**, 4745–4756 (2004).
[24]M. Yamazaki, S. Sato, H. Ashida, D. Saito, Y. Okada, and M. Obara, "Measurement of burn depths in rats using multiwavelength photoacoustic depth profiling," J. Biomed. Opt. **10**, 064011–064014 (2005).
[25]X. Wang, Y. Xu, M. Xu, S. Yokoo, E. S. Fry, and L. V. Wang, "Photoacoustic tomography of biological tissues with high cross-section resolution: Reconstruction and experiment," Med. Phys. **29**, 2799–2805 (2002).
[26]A. Villringer and B. Chance, "Non-invasive optical spectroscopy and imaging of human brain function," Trends Neurosci. **20**, 435–442 (1997).
[27]R. D. Hoge, J. Atkinson, B. Gill, G. R. Crelier, S. Marrett, and G. B. Pike, "Investigation of BOLD signal dependence on cerebral blood flow and oxygen consumption: The deoxyhemoglobin dilution model," Magn. Reson. Med. **42**, 849–863 (1999).

[28]S. Ogawa, D. W. Tank, R. Menon, J. M. Ellermann, S. G. Kim, H. Merkle, and K. Ugurbil, "Intrinsic signal changes accompanying sensory stimulation: Functional brain mapping with magnetic resonance imaging," Proc. Natl. Acad. Sci. U.S.A. **89**, 5951–5955 (1992).
[29]A. Grinvald, R. D. Frostig, E. Lieke, and R. Hildesheim, "Optical imaging of neuronal activity," Physiol. Rev. **68**, 1285–1366 (1988).
[30]X. Wang, Y. Pang, G. Ku, X. Xie, G. Stoica, and L. V. Wang, "Noninvasive laser-induced photoacoustic tomography for structural and functional *in vivo* imaging of the brain," Nat. Biotechnol. **21**, 803–806 (2003).
[31]R. A. Kruger, W. L. Kiser, D. R. Reinecke, G. A. Kruger, and K. D. Miller, "Thermoacoustic computed tomography-technical considerations," Mol. Imaging **2**, 113–123 (2003).
[32]J. A. McPherson, K. G. Barringhaus, G. G. Bishop, J. M. Sanders, J. M. Rieger, S. E. Hesselbacher, L. W. Gimple, E. R. Powers, T. Macdonald, G. Sullivan, J. Linden, and I. J. Sarembock, "Adenosine A(2A) receptor stimulation reduces inflammation and neointimal growth in a murine carotid ligation model," Arterioscler., Thromb., Vasc. Biol. **21**, 791–796 (2001).
[33]S. Vorstrup, B. Brun, and N. A. Lassen, "Evaluation of the cerebral vasodilatory capacity by the acetazolamide test before EC-IC bypass surgery in patients with occlusion of the internal carotid artery," Stroke **17**, 1291–1298 (1986).
[34]F. Chollet, P. Celsis, M. Clanet, B. Guiraud-Chaumeil, A. Rascol, and J. P. Marc-Vergnes, "SPECT study of cerebral blood flow reactivity after acetazolamide in patients with transient ischemic attacks," Stroke **20**, 458–464 (1989).
[35]E. Hojer-Pedersen, "Effect of acetazolamide on cerebral blood flow in subacute and chronic cerebrovascular disease," Stroke **18**, 887–891 (1987).
[36]S. Vorstrup, L. Henriksen, and O. B. Paulson, "Effect of acetazolamide on cerebral blood flow and cerebral metabolic rate for oxygen," J. Clin. Invest. **74**, 1634–1639 (1984).
[37]A. Hauge, G. Nicolaysen, and M. Thoresen, "Acute effects of acetazolamide on cerebral blood flow in man," Acta Physiol. Scand. **117**, 233–239 (1983).
[38]J. K. Barton, G. Frangineas, H. Pummer, and J. F. Black, "Cooperative phenomena in two-pulse, two-color laser photocoagulation of cutaneous blood vessels," Photochem. Photobiol. **73**, 642–650 (2001).
[39]X. Wang, X. Xie, G. Ku, L. V. Wang, and G. Stoica, "Noninvasive imaging of hemoglobin concentration and oxygenation in the rat brain using high-resolution photoacoustic tomography," J. Biomed. Opt. **11**, 024015–024023 (2006).
[40]Z. Yuan and H. B. jiang, "Quantitative photoacoustic tomography: Recovery of optical absorption coefficient maps of heterogeneous media," Appl. Phys. Lett. **88**, 231101–231103 (2006).
[41]Z. Yuan, Q. Z. Zhang, and H. B. Jiang, "Simultaneous reconstruction of acoustic and optical properties of heterogeneous media by quantitative photoacoustic tomography," Opt. Express **14**, 6749–6754 (2006).
[42]A. Grinvald, R. D. Frostig, R. M. Siegel, and E. Bartfeld, "High-resolution optical imaging of functional brain architecture in the awake monkey," Proc. Natl. Acad. Sci. U.S.A. **88**, 11559–11563 (1991).
[43]R. D. Frostig, E. E. Lieke, D. Y. Ts'o, and A. Grinvald, "Cortical functional architecture and local coupling between neuronal activity and the microcirculation revealed by *in vivo* high-resolution optical imaging of intrinsic signals," Proc. Natl. Acad. Sci. U.S.A. **87**, 6082–6086 (1990).
[44]G. Wang, K. Tanaka, and M. Tanifuji, "Optical imaging of functional organization in the monkey inferotemporal cortex," Science **272**, 1665–1668 (1996).
[45]D. Yang, D. Xing, Y. Tan, H. Gu, and S. Yang, "Integrative prototype B-scan photoacoustic tomography system based on a novel hybridized scanning head," Appl. Phys. Lett. **88**, 174101–174103 (2006).
[46]D. Yang, D. Xing, H. Gu, and L. Zeng, "Fast multielement phase-controlled photoacoustic imaging based on limited-field-filtered back-projection algorithm," Appl. Phys. Lett. **87**, 194101–194103 (2005).
[47]X. Wang, G. Ku, M. A. Wegiel, D. J. Bornhop, G. Stoica, and L. V. Wang, "Noninvasive photoacoustic angiography of animal brains *in vivo* with near-infrared light and an optical contrast agent," Opt. Lett. **29**, 730–732 (2004).
[48]Y. Wang, X. Xie, X. Wang, G. Ku, K. L. Gill, D. P. O'Neal, G. Stoica, and L. V. Wang, "Photoacoustic tomography of a nanoshell contrast agent in the *in vivo* rat brain," Nano Lett. **4**, 1689–1693 (2004).